Interface and defect structures of Zn–ZnO core–shell heteronanobelts

Y. Ding, X. Y. Kong, and Z. L. Wang[a)]
School of Materials Science and Engineering, Georgia Institute of Technology, Atlanta, Georgia 30332-0245

(Received 25 July 2003; accepted 19 October 2003)

Interface and defect structures of Zn–ZnO core–shell nanobelts have been investigated using high-resolution transmission electron microscopy. Most of the nanobelts can be classified into two types from their growth directions: $[2\bar{1}\bar{1}0]$ and [0001], with the top/bottom surfaces being (0001) and $(2\bar{1}\bar{1}0)$, respectively. The Zn core and ZnO shell overlapped areas display a two-dimensional moiré pattern resulting from the lattice mismatch. In the $\langle 2\bar{1}\bar{1}0\rangle$ growth nanobelts, a network of three sets of misfit dislocations relaxes the mismatch strain in the top/bottom interfaces, and every set rotates 60° with respect to the other; there are two types of grains oriented in specific orientations that compose the side wall of the ZnO shell. In the [0001] growth nanobelts, a network containing a set of stacking faults in (0001) planes and a set of misfit dislocations in $(01\bar{1}0)$ planes takes the main role in the misfit relaxation. Threading dislocations indicated by terminating moiré fringes are present in both of them, which are located at the small angle rotated boundary between adjacent misoriented ZnO grains. © *2004 American Institute of Physics.* [DOI: 10.1063/1.1632017]

I. INTRODUCTION

One-dimensional nanomaterials, especially, the coaxial nanomaterials composed of semiconducting, insulating, or metallic materials in the radial direction have attracted much attention in recent years due to their potential applications in fabricating nanometer-scale electronic devices possessing various interesting functions.[1,2] ZnO, which is widely used as a transparent conducting oxide material, optical devices and gas sensors, is a good candidate for one-dimensional nanomaterials.[3] After fabricating ZnO nanotubes, nanowires and nanobelts,[4,5] recently, metal–semiconductor core–shell Zn–ZnO nanobelts and nanowires have been synthesized.[6–10] From simple structure analysis, we know that the Zn core and the sheathing ZnO shell have an epitaxial relationship.[6] Considering the large difference between their lattice parameters,[11] the misfit relaxation in the core–shell interface is of great scientific interest. As we know from two-dimensional materials, such as semiconductor, ferroelectrics thin films,[12–14] the interface plays a key role in their properties. In order to use metal–semiconductor Zn–ZnO core–shell nanobelts as devices, the detailed structure, especially how to relax the large misfit, must first be understood.

Nanobelt is a quasione-dimensional nanomaterial, which has a rectangular cross section with a specific growth direction, side surfaces, and top/bottom surfaces. Their geometrical shape is very uniform with atomically flat surfaces. The most typical examples are the transparent conducting oxides, such as ZnO, SnO_2, In_2O_3 and CdO.[5] The nanobelt of a monocrystal structure is free from dislocations but planar defects, such as twins and stacking faults, have been observed.[15]

In this work, we investigate the microstructure of the Zn–ZnO core–shell structured nanobelts in detail using transmission electron microscopy (TEM). The belts can be classified into two types from their growth directions: along $[2\bar{1}\bar{1}0]$ with top/bottom surfaces (0001) and along [0001] with top/bottom surface $(2\bar{1}\bar{1}0)$. Network defect structures have been found in both types of nanobelts to relax the misfit strain. The network in $[2\bar{1}\bar{1}0]$ growth nanobelts contains three sets of misfit dislocations with 60° angles among them; while the [0001] growth belts contain a set of misfit dislocations and a set of stacking faults with 90° angles between them. Threading dislocations have also been observed in them, which are located at the small angle rotated boundary between adjacent misoriented ZnO grains.

II. RESULTS AND DISCUSSION

For this study, the Zn–ZnO core–shell nanobelts were synthesized with a kinetic controlled process using a solid–vapor phase deposition system; the detail process was reported elsewhere.[6] The samples are transferred onto carbon film coated grids. The high-resolution TEM (HRTEM) work was carried out at 400 kV using a JEOL-4000EX.

In the Zn–ZnO nanobelts we fabricated, their preferred growth directions are along $[2\bar{1}\bar{1}0]$ and [0001], and taking (0001) and $(2\bar{1}\bar{1}0)$ planes as their top/bottom surfaces, respectively. We will describe the microstructures of these two types of nanobelts separately below.

A. The $[2\bar{1}\bar{1}0]$ growth nanobelts

A low-magnification image of the $[2\bar{1}\bar{1}0]$ growth nanobelts is illustrated in Fig. 1(a). Typical zig-zag structures are frequently observed in this type of nanobelt, which are due to a change of the growth direction from $[2\bar{1}\bar{1}0]$ to $[\bar{1}2\bar{1}0]$, two crystallographically equivalent directions. The uniform contrast of the nanobelt in Fig. 1(a) also indicates that it has a belt shape with a width around 60 nm. The selected-area electron diffraction pattern of the nanobelt is shown in Fig.

a)Author to whom correspondence should be addressed; electronic mail: zhong.wang@mse.gatech.edu

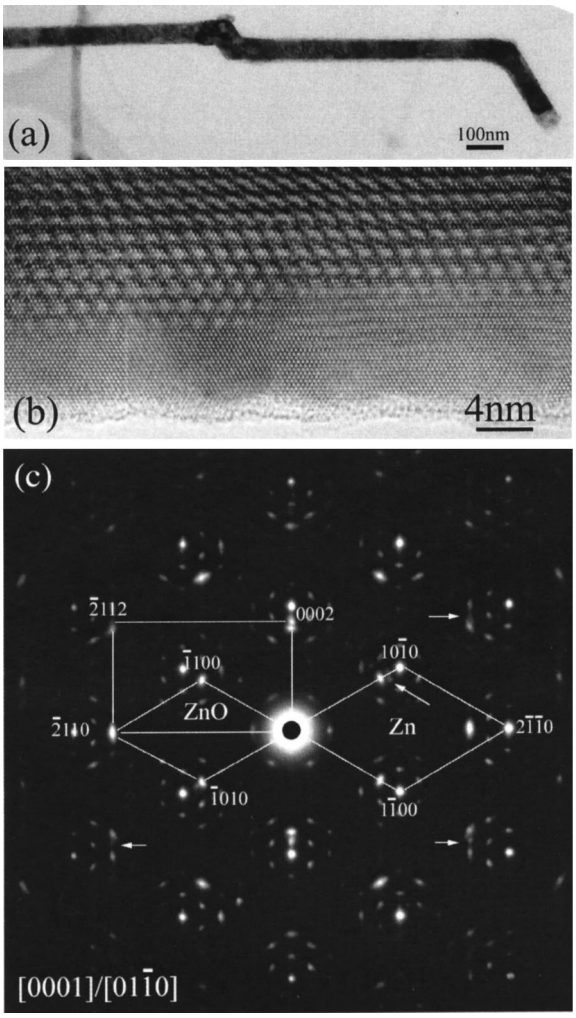

FIG. 1. (a) Low-magnification and (b) high-resolution TEM images of a $[2\bar{1}\bar{1}0]$ growth Zn–ZnO core–shell nanobelt, respectively; and (c) selected-area electron diffraction pattern from the nanobelt in (a) and (b).

1(c), where satellite spots appear around the basic reflections of Zn and ZnO due to double diffraction. The diffraction pattern indicates that the core Zn and sheath ZnO have an epitaxial relationship with an identical orientation, the existence of the extra reflections as (0002) and $(\bar{2}112)$ will be discussed in detail later.

Figure 1(b) shows a HRTEM image from a part of the nanobelt in Fig. 1(a). The downside is just the sheathing ZnO (0001) lattice image, which is about 6 nm in width; the upside of the image depicts a two-dimensional moiré pattern with electron beam parallel to the *c* axes of the two overlapping Zn and ZnO lattices. Considering that a fringe moiré pattern is produced by a single set of parallel overlapping lattice planes of Zn and ZnO, there are three intersecting moiré fringes; every individual pattern is rotated with respect to the other by 60°, appearing in the moiré pattern in Fig. 1(b). This is due to the epitaxial orientation between Zn and ZnO as well as the zone axis incidence of the electron beam.

The spacing of the moiré fringes is given by[16]

$$D=\frac{d_{\text{core}}d_{\text{shell}}}{|d_{\text{shell}}-d_{\text{core}}|}, \tag{1}$$

where d_{core} and d_{shell} are the corresponding *d* spacing of the overlapping planes for the Zn core and ZnO shell. Taking into account that the lattice parameters of Zn and ZnO are $a=0.2665$ nm, $c=0.4947$ nm and $a=0.3249$ nm, $c=0.5206$ nm, respectively, the *D* spacing of the $\{0\bar{1}10\}$ moiré fringes should be 1.30 nm, which corresponds to one moiré fringe every 4.6 atomic planes of ZnO or 5.6 atomic planes of Zn. Consequently, in a stress-free configuration, moiré fringes should take the above value, which is almost the same as our experimental observation. The natural misfit *m* between the two lattices is[17]

$$m=\frac{|d_{\text{shell}}-d_{\text{core}}|}{d_{\text{core}}}, \tag{2}$$

taking Zn core as the reference crystal, $m=21.6\%$ in this case. The mismatch between the Zn core and ZnO shell could be relaxed by a network of misfit dislocations introduced in the plane of the interface. Since both crystals belong to the hexagonal crystal system, the misfit dislocation network in the (0001) plane consists of three equivalent sets of perfect dislocations. The Burgers vector of the misfit dislocations corresponds to $b=1/3\langle 2\bar{1}\bar{1}0\rangle$ in term of the Zn lattice. The spacing between misfit dislocations is given as

$$D_d=\frac{|b|}{m}. \tag{3}$$

The dislocation spacing is about 1.23 nm, which is approximate to the moiré fringe spacing. At the same time, the operating reciprocal lattice vectors of the $\{0\bar{1}\bar{1}0\}$ Zn and ZnO lattice planes are perpendicular to the direction of the dislocation lines. Thus, the image of the moiré pattern and the misfit dislocation network should be in correspondence. In Fig. 2(a) a HRTEM image of the moiré fringe pattern, the sharp contrast projected atomic columns, indicates regions of good fits, while the blurred contrast comes from regions of poorer fit, where misfit dislocations are located. Using only one set of parallel Fourier spatial frequencies $[(0\bar{1}\bar{1}0)$ for Zn and ZnO], we get a Fourier filtered image of Fig. 2(a), as given in Fig. 2(b). The white lines mark the poorer fit regions, which are the positions of one set of misfit dislocations. The arrowheads point out the positions where three misfit dislocations, with 60° between two of them, meet. There are 4–5 atomic $(0\bar{1}\bar{1}0)$ planes between the two nearby misfit dislocations, as expected from the above calculation.

Figures 3(a) and 3(b) are low-magnification and high-magnification dark-field images using a set of Zn and ZnO $(0\bar{1}\bar{1}0)$ reflections, which show a single moiré fringe pattern. The occurrence of threading dislocations pointed out by white arrows in Fig. 3(b) is readily deduced from the terminating moiré fringes. The formation of the threading dislocations could be attributed to the slight rotation between the adjacent misoriented ZnO islands at the early stage of the sheath formation, similar to the interface dislocations at a small angle rotation boundary.

It is worth noticing that there are some extra reflections in Fig. 1(c), which are not due to double diffraction among the reflections of Zn and ZnO perpendicular to the incident beam direction [0001]. After measuring the corresponding

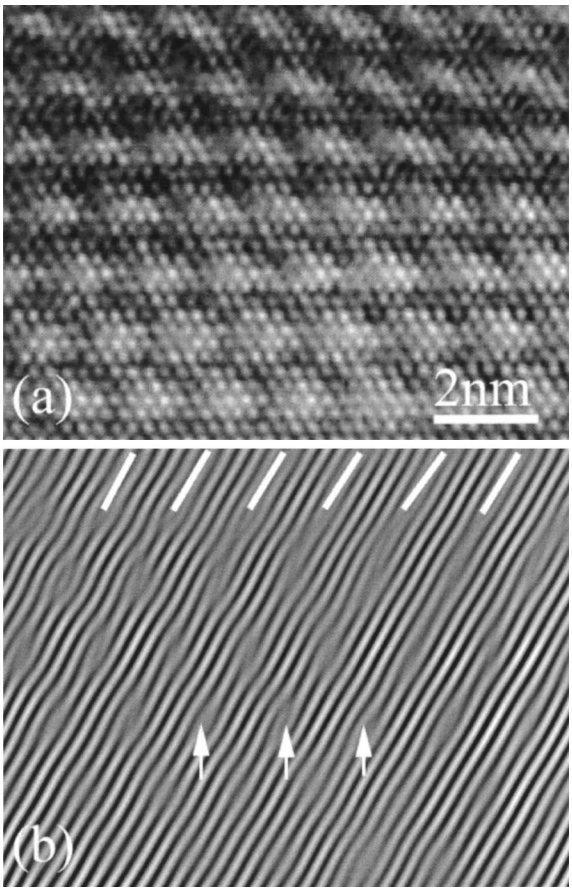

FIG. 2. (a) [0001] viewed HRTEM image of the $[2\bar{1}\bar{1}0]$ growth nanobelt, depicting the two-dimensional moiré fringe pattern; and (b) Fourier filtered image of (a). White lines indicate the locations of misfit dislocations.

lengths and the angles between them, the fundamental spot indicated by the rectangular frame is the $[0110]$ diffraction pattern of ZnO. Therefore, there exist two kinds of epitaxial relationship between the core Zn and the sheathing ZnO: one takes the relationship as $[2\bar{1}\bar{1}0]_{Zn}\|[2\bar{1}\bar{1}0]_{ZnO}$, $(0001)_{Zn}\|(0001)_{ZnO}$, another as $[2\bar{1}10]_{Zn}\|[2\bar{1}10]_{ZnO}$,

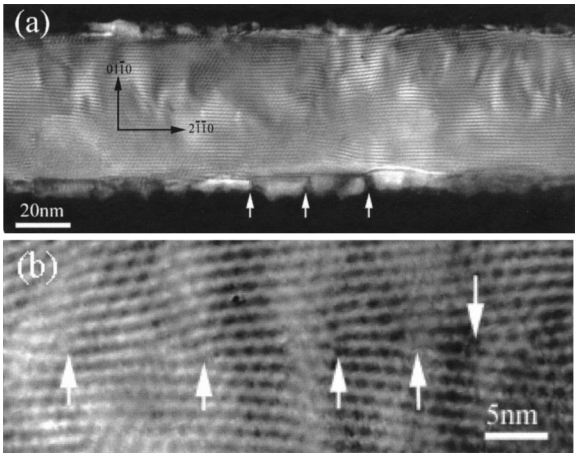

FIG. 3. (a) Low-magnification and (b) high-magnification dark-field images recorded from the $[2\bar{1}10]$ growth nanobelt, using one set of Zn and ZnO (0110) reflections. White arrowheads point out the locations of threading dislocations.

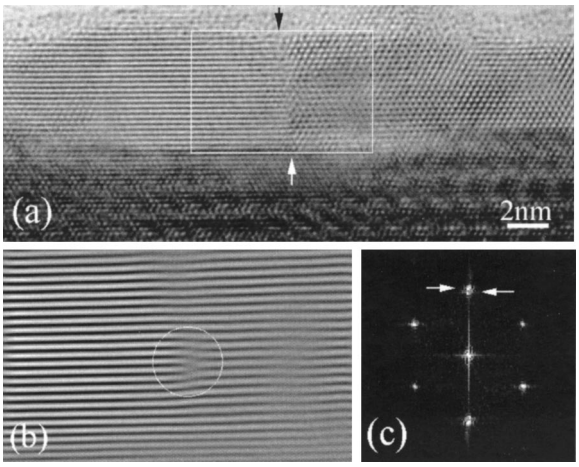

FIG. 4. (a) Two nearby grains taking $[2\bar{1}\bar{1}0]_{Zn}\|[2\bar{1}\bar{1}0]_{ZnO}$, $(0001)_{Zn}\|(0001)_{ZnO}$ and $[2\bar{1}10]_{Zn}\|[2\bar{1}10]_{ZnO}$, $(0001)_{Zn}\|(0110)_{ZnO}$ epitaxial relationship with the Zn core; (b) Fourier filtered image from the white rectangle closed area in (a), showing a dislocation at the grain boundary; and (c) Fourier transform from the solid rectangle closed area.

$(0001)_{Zn}\|(01\bar{1}0)_{ZnO}$. If so, considering the formula of Eq. (2), the second kind of epitaxial relationship means a smaller mismatch, just 12.7% along the $[0001]_{Zn}$ direction (it is 21.6% in the first case), which are matched with the $[0110]_{ZnO}$. There are also two sets of (0110)* reflections present in Fig. 1(c) with 60° rotation between them [seeing the extra reflection in the middle of Zn and ZnO (1010)]. They are due to the zig-zag form of the nanobelts as presented in Fig. 1(a).

The indirect evidence of the existence of the second epitaxial relationship can be confirmed in the HRTEM image presented in Fig. 4(a) viewed along $[0001]_{Zn}$. Compared with the lattice image in the right part, only fringes appear in the left, which suggests that they belong to two separated grains. Fourier transform from the area enclosed by the white solid rectangle is shown in Fig. 4(c). The spatial frequencies corresponding to the horizontal planes of both sides are not the same, which are emphasized by two arrowheads. They could be indexed as $(0002)_{ZnO}$ and $(0110)_{ZnO}$, the same as the case in Fig. 1(c). The filtered image using these two spatial frequencies is shown in Fig. 4(b). A dislocation exists in the boundary between the two grains, which also suggests the difference between the spacing of the two lattice planes. The reason why only fringes appear in the left grain is due to the microscope resolution that is not good enough to resolve the $(2\bar{1}10)$ planes of 0.16 nm in spacing. From the dark-field image in Fig. 3(a), the shell layer is separated into several parts by the white arrowheads, and each part is around 20 nm in length. The HRTEM images from these parts indicate that they are the same case as shown in Fig. 4. It indicates that grains, in alternating epitaxial relationships, compose the shell ZnO.

B. The [0001] growth nanobelts

Figure 5(a) is a dark-field image, which illustrates a nanobelt growing along [0001] with the top/bottom surface as $(2\bar{1}10)$. The selected-area diffraction pattern of the nano-

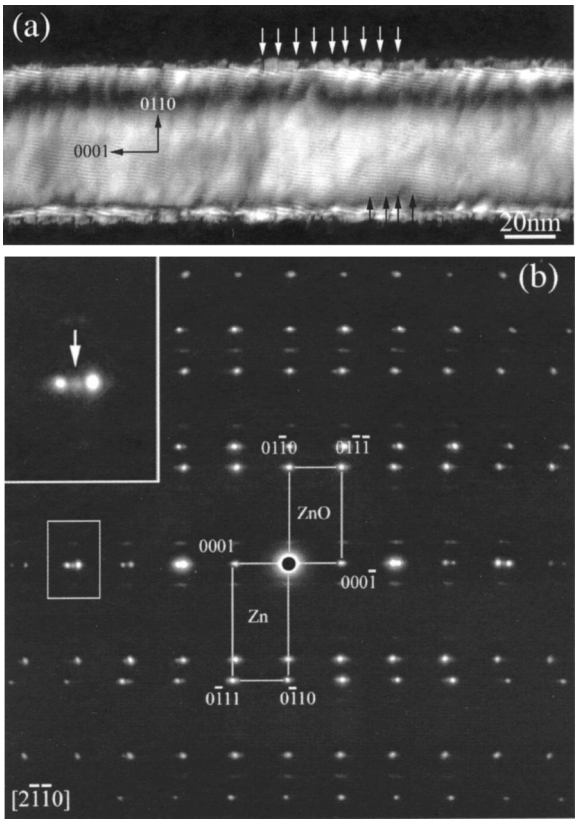

FIG. 5. (a) Dark-field image of a [0001] growth nanobelt; the white arrowheads in upside of the images indicate the locations of stacking faults; and (b) selected-area diffraction pattern of the nanobelt in (a). The rectangle-enclosed area in (b) is magnified in the inset.

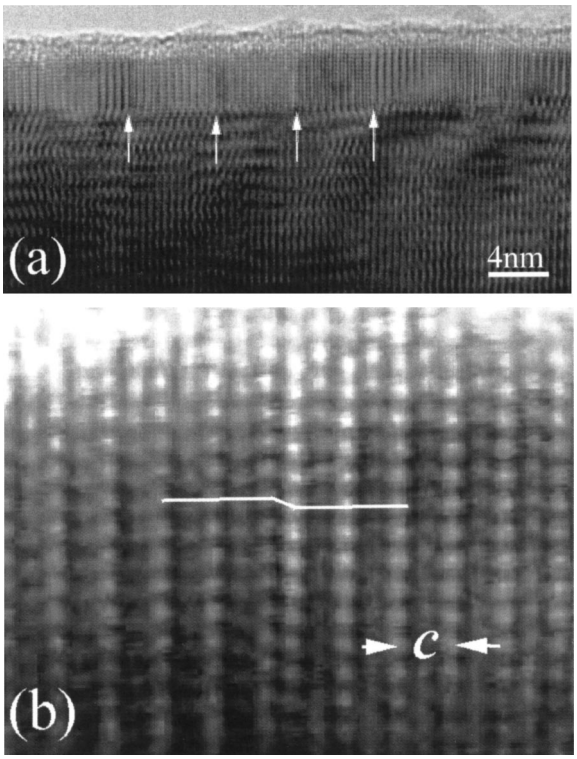

FIG. 6. (a) Low-magnification and (b) high-magnification HRTEM images of the I_1 stacking fault in the Fig. 5 depicted nanobelt.

belts is shown in Fig. 5(b), which indicates an epitaxial relationship between Zn core and ZnO shell: $[0110]_{Zn}\|[0110]_{ZnO}$, $(2110)_{Zn}\|(2110)_{ZnO}$.

As mentioned in the above section, a network of three sets of misfit dislocations in the main facet (0001) plane relaxes the mismatch in the [2110] growth nanobelts. Turning to [0001] growth nanobelts, the main facet changes to (2110) plane. The mismatches along the two main directions of [0001] and [0110] in this plane are $m_c=5.2\%$ and $m_{01\bar{1}0}=21.6\%$, respectively. If the misfit dislocations are still the mechanism to relax mismatch strain, the spacing of the misfit dislocations along [0110] should be the same as 1.23 nm as the nanobelts discussed above, but it will be 9.51 nm along the [0001] direction for the Burgers of the misfit dislocations being [0001]. Below, we will focus on the mismatch relaxation forms from these two directions.

Regular defect arrays as pointed out by the small white arrowheads in Fig. 5(a), exist in the ZnO shell, and cross the whole belt (as dark arrows marked). They cannot be misfit dislocations. A low-magnification HRTEM image containing these defects is recorded in Fig. 6(a). The lattice image indicates that the defects are I_1 intrinsic stacking faults.[18] The Fourier filtered image of one stacking fault in Fig. 6(b) depicts the translation of $R=R_c+R_{01\bar{1}0}=1/2[0001]+1/3[0110]$ crossing the defect. It indicates that the formation of stacking faults in (0001) planes may take a role in the misfit relaxation along [0001] direction. Supposing the mismatch strain is fully relaxed by the stacking fault arrays, the spacing D_{st} between two stacking faults should be

$$D_{st}=\frac{R_c}{m_c}. \tag{4}$$

It is 5.01 nm, about 9–10 atomic planes of ZnO, which are close to the results of 5–6 nm as we measured from Figs. 5(a) and 6(a). It is just half of the predicted misfit dislocation spacing. At the same time, the stacking faults arrange regularly, superlattice reflections should appear in the selected-area diffraction pattern. Examining Fig. 5(b) carefully, these reflections do exist (as indicated by small white arrowheads in the inset). One of them is located in the middle position of Zn and ZnO (0004) reflections. They correspond to the spacing of 5.27 nm. Therefore, the stacking fault arrays take the key roles in the misfit relaxation in the [0001] direction.

Figure 7(a) is a HRTEM image recorded from the Zn and ZnO overlapping area of the [0001] growth nanobelt. Filtered images in Figs. 7(b) and 7(c) are obtained by applying Fourier transforms to the HRTEM image of Fig. 7(a), which use only the parallel Fourier spatial frequencies corresponding to the (0001) and $(01\bar{1}0)$ planes, respectively. The large white arrowheads in Fig. 7(b) point out the locations of the stacking faults, while the small white arrowheads in Fig. 7(c) point out the misfit dislocations in $(01\bar{1}0)$ planes. The shift between the misfit dislocations in [0110] directions is due to the displacement of the stacking faults in the middle of them. Thus it is clear that the network of misfit dislocations and stacking faults relaxes the mismatch in the [0001] growth core–shell nanobelts.

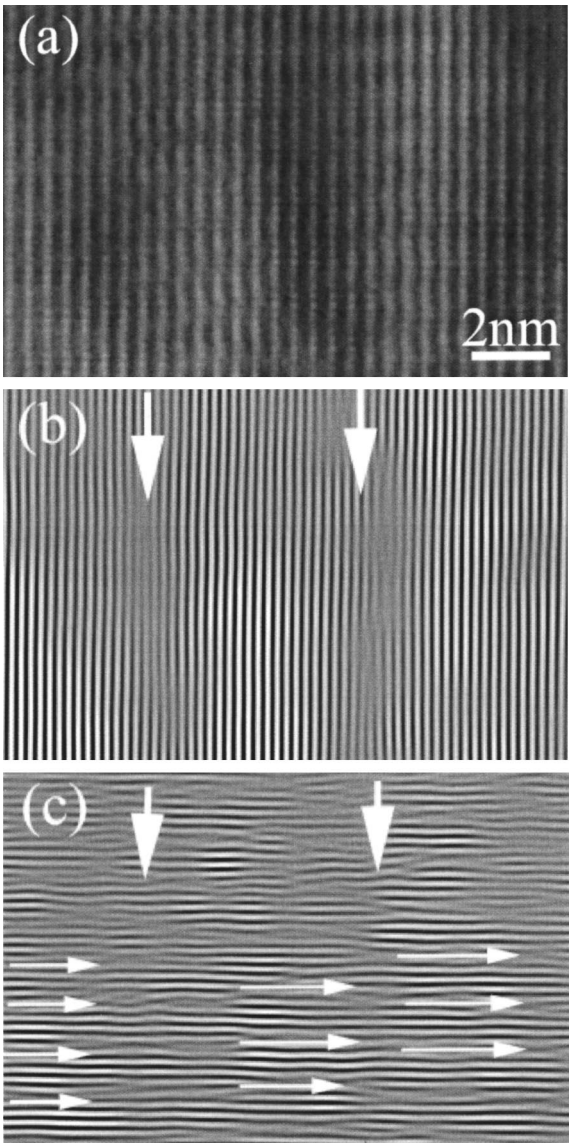

FIG. 7. (a) HRTEM image of a [0001] growth nanobelt recorded from the Zn–ZnO overlapping area; (b) and (c) Fourier filtered images of (a) using the parallel Fourier spatial frequencies corresponding to Zn and ZnO (0001) and $(01\bar{1}0)$ planes, respectively. Stacking faults indicated by large arrowheads; misfit dislocations indicated by small arrowheads.

Figure 8 is a dark-field image using the Zn and ZnO $(01\bar{1}0)$ reflections. As the case in $[2\bar{1}\bar{1}0]$ growth nanobelts, the existence of the threading dislocations is also suggested from the terminating of moiré fringes (shown inside the areas indicated by white circles). The contrast of the stacking faults in Figs. 5 and 6 can also be observed in Fig. 8, as indicated by white arrowheads.

III. CONCLUSION

Lattice mismatch relaxation mechanisms in the core–shell Zn–ZnO nanobelt structure have been investigated in detail using transmission electron microscopy. In the $[2\bar{1}\bar{1}0]$ growth nanobelts, a network containing three sets of misfit dislocations, where every set rotates 60° with respect to the other, relaxes the mismatch in the (0001) interfaces. Two kinds of epitaxial relationship have been found in the side surfaces of the nanobelts, which are $[2\bar{1}\bar{1}0]_{Zn}\|[2\bar{1}\bar{1}0]_{ZnO}$, $(0001)_{Zn}\|(000\bar{1})_{ZnO}$, and $[2\bar{1}\bar{1}0]_{Zn}\|[2\bar{1}\bar{1}0]_{ZnO}$, $(0001)_{Zn}\|(01\bar{1}0)_{ZnO}$. One by one ZnO grains following these two epitaxial relationships compose the side shell of the nanobelt. In another [0001] growth nanobelt, a network of misfit dislocations and stacking faults with 90° between them takes the key role in the misfit relaxation. Threading dislocations are observed in both types of nanobelts, which might be attributed to a small rotation boundary between the adjacent misoriented ZnO grains.

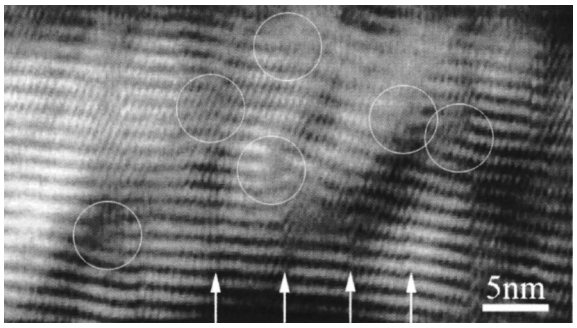

FIG. 8. Dark field indicates the existence of threading dislocations in [0001] growth nanobelt. White arrowheads indicate stacking faults.

ACKNOWLEDGMENT

This work is supported by NSF Grant No. ECS-0210332.

[1] K. Suenaga, C. Colliex, N. Demoncy, A. Loiseau, H. Pascard, and F. Willaime, Science **278**, 653 (1997).
[2] Y. Zhang, K. Suenaga, C. Colliex, and S. Iijima, Science **281**, 973 (1998).
[3] L. Vayssieres, K. Keis, A. Hagfeldt, and S.-E. Lindquist, Chem. Mater. **13**, 4386 (2001).
[4] P. D. Yang *et al.*, Adv. Funct. Mater. **12**, 323 (2002).
[5] Z. W. Pan, Z. R. Dai, and Z. L. Wang, Science **291**, 1947 (2001).
[6] X. Y. Kong, Y. Ding, and Z. L. Wang, J. Phys. Chem. (in press).
[7] J. Wu, S. Liu, C. Wu, K. Chen, and L. Chen, Appl. Phys. Lett. **81**, 1312 (2002).
[8] J. Q. Hu, Y. Bando, and Z. W. Liu, Adv. Mater. (Weinheim, Ger.) **12**, 1000 (2003).
[9] J. Q. Hu, Q. Li, X. M. Meng, C. S. Lee, and S. T. Lee, Chem. Mater. **15**, 305 (2003).
[10] Y. F. Yan, P. Liu, M. J. Romero, and M. M. Al-Jassim, J. Appl. Phys. **93**, 4807 (2003).
[11] F. Gallaso, *Structure and Properties of Inorganic Solids* (Pergamon, New York, 1970).
[12] Th. Kehagias, Ph. Komninou, G. Nouet, P. Ruterana, and Th. Karakostas, Phys. Rev. B **64**, 195329 (2001).
[13] N. Y. Jin-Phillipp, W. Sigle, A. Black, D. Babic, J. E. Bowers, E. L. Hu, and M. Rühle, J. Appl. Phys. **89**, 1017 (2001).
[14] L. Ryen, E. Olsson, L. D. Madsen, X. Wang, C. N. L. Edvardsson, S. N. Jacobsen, U. Helmersson, S. Rudner, and L.-D. Wernlund, J. Appl. Phys. **83**, 4884 (1998).
[15] Z. L. Wang, Z. W. Pan, and Z. R. Dai, Microsc. Microanal. **8**, 467 (2002).
[16] P. B. Hirsch, A. Howie, R. B. Nicholson, D. W. Pashley, and M. J. Whelan, *Electron Microscopy of Thin Crystals* (Butterworths, London, 1965).
[17] J. W. Matthews, *Dislocations in Solids* (North-Holland, Amsterdam, 1979), Vol. 2.
[18] V. Potin, P. Ruterana, and G. Nouet, J. Phys.: Condens. Matter **12**, 10301 (2000).